Engineering 19 (2022) 93–104

Contents lists available at ScienceDirect

Engineering

journal homepage: www.elsevier.com/locate/eng

Research
Civil Engineering Materials—Article

Vibration Serviceability of Large-Span Steel–Concrete Composite Beam with Precast Hollow Core Slabs Under Walking Impact

Jiepeng Liu [a], Shu Huang [b], Jiang Li [a,*], Y. Frank Chen [a,c]

[a] School of Civil Engineering & Key Laboratory of New Technology for Construction of Cities in Mountain Area, Ministry of Education, Chongqing University, Chongqing 400045, China
[b] Central-South Architectural Design Institute Co., Ltd., Wuhan 430071, China
[c] Department of Civil Engineering, The Pennsylvania State University, PA 17057, USA

ARTICLE INFO

Article history:
Received 29 September 2020
Revised 28 February 2021
Accepted 6 April 2021
Available online 6 August 2021

Keywords:
Composite beam
Hollow core slab
Walking force
Floor vibration
Mode shape

ABSTRACT

A large-span steel–concrete composite beam with precast hollow core slabs (CBHCSs) is a relatively new floor structure that can be applied to various long-span structures. However, human-induced vibrations may present serviceability issues in such structures. To alleviate vibrations, both the walking forces excited by humans and the associated floor responses must be elucidated. In this study, 150 load–time histories of walking, excited by 25 test participants, are obtained using a force measuring plate. The dynamic loading factors and phase angles in the Fourier series functions for one-step walking are determined. Subsequently, walking tests are performed on seven CBHCS specimens to capture the essential dynamic properties of mode shapes, natural frequencies, damping ratios, and acceleration time histories. The CBHCS floor system generally exhibits a high frequency (> 10 Hz) and low damping (damping ratio < 2%). Sensitivity studies using the finite element method are conducted to investigate the vibration performance of the CBHCS floor system, where the floor thickness, steel beam type, contact time, and human weight are considered. Finally, analytical expressions derived for the fundamental frequency and peak acceleration agree well with the experimental results and are hence proposed for practical use.

1. Introduction

A relatively new steel–concrete composite beam using precast hollow core slabs (CBHCSs), as shown in Fig. 1(a), is proposed herein. Compared with previous composite beams, such new composite beams offer the following advantages: ① The CBHCSs can extend the structural span owing to the lighter mass of the hollow core slab (HCS); ② both the steel beam and precast HCS can be prefabricated in a shop, thereby obviating significant amounts of on-site wet work; ③ the integrity, strength, and stiffness are improved significantly, and water leakages are alleviated owing to the use of cast-in-place (CIP) concrete on the precast HCS; and ④ cracks on the floor surface are avoided owing to the mesh bars configured in the CIP concrete layer. This study focused only on the composite beam highlighted in the dashed area shown in Fig. 1(a). Therefore, only this region of the floor was represented in the experiments and finite element (FE) simulations.

Studies pertaining to shear behavior [1,2], flexural behavior [3–9], thermal performance, and fire performance [10,11] have been conducted. Although the HCS is light and can stretch the structural span, its longer floor system is likely to experience vibrations from human activities [12–14]. In fact, the vibrational behavior of this relatively new composite beam system should be further investigated, as studies pertaining to it are scarce.

To alleviate the abovementioned vibration problem, the walking forces excited by humans must be elucidated. Harper [15] performed walking tests, investigated the mechanics of walking, and proposed an M-shaped forcing function. Blanchard et al. [16] defined the walking force function (vertical force F_{vertical} and horizontal force F_{lateral}) using the Fourier series as follows:

$$F_{\text{vertical}}(t) = G + G\sum_{i=1}^{n} \alpha_{\text{vertical }i} \sin(2i\pi f_{\text{p}} t - \varphi_{\text{vertical }i}) \tag{1}$$

$$F_{\text{lateral}}(t) = G\sum_{i=1}^{n} \alpha_{\text{lateral }i} \sin(i\pi f_{\text{p}} t - \varphi_{\text{lateral }i}) \tag{2}$$

* Corresponding author.
E-mail address: lijiangcqu@cqu.edu.cn (J. Li).

https://doi.org/10.1016/j.eng.2021.04.025

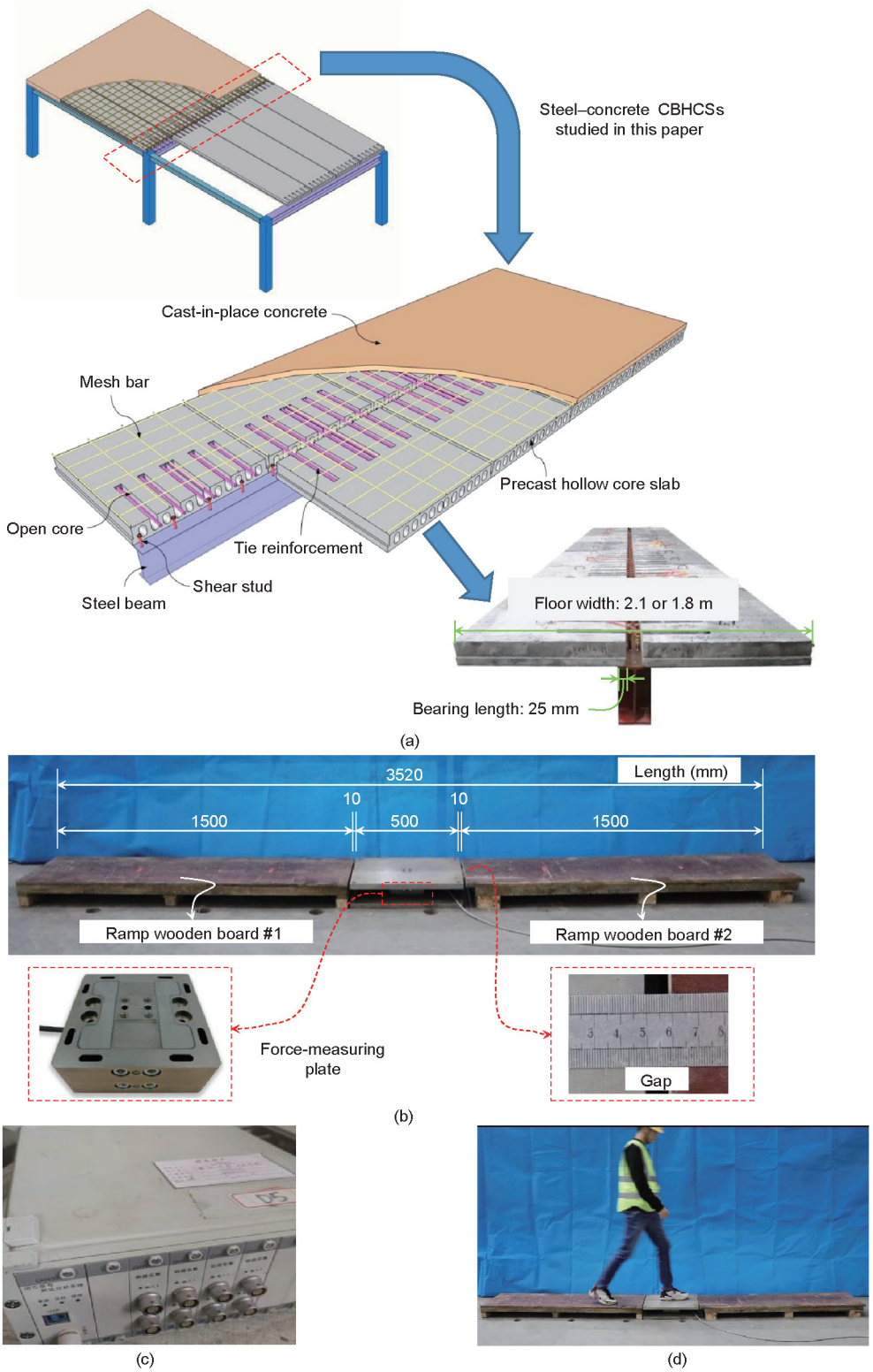

Fig. 1. (a) Details of CBHCSs; (b, c) the monitoring system, including the force-measuring plate (ME-K3D160, Germany) and the data acquisition system (DH5922N, Jiangsu Donghua Testing Technology Co., Ltd., China); and (d) the field test.

where G is the human weight (N); i is the ith harmonic; t is the time; $\alpha_{\text{vertical } i}$ and $\alpha_{\text{lateral } i}$ are the vertical and horizontal coefficients of the Fourier series, respectively; $\varphi_{\text{vertical } i}$ and $\varphi_{\text{lateral } i}$ are the vertical and horizontal phase angles of the Fourier series, respectively; f_p is the stride rate; and n is the total number of contributing harmonics.

The duration of single-step excitation T_p is an important vibration parameter. It begins when the footfall touches the measuring force plate and ends when the footfall leaves the plate completely. T_p reflects the walking pace. In previous studies [17–20], the stride rate f_p was used to determine the dynamic loading factors (DLFs) for the walking pace function using the Fourier series. However,

few studies have been conducted to relate the DLFs with T_p based on the simulation of a walking model.

The objectives of this study are as follows:

(1) To establish the Fourier series forcing function with T_p for one-step walking experimentally;

(2) To analyze the data measured from steady-state walking movements and establish the dynamic characteristics of the CBHCS;

(3) To conduct a sensitivity study using the finite element method;

(4) To derive and propose analytical expressions for the fundamental frequency and peak acceleration of a CBHCS system.

2. Measurement of walking forces

2.1. Experimental plan

The monitoring system comprised a measuring device (Fig. 1(b)) and a data acquisition system (Fig. 1(c)). The measuring device was a custom-designed force-measuring plate system with a total length of 3520 mm, including one force plate (500 mm long), two ramp wooden boards (1500 mm long each), and two 10 mm gaps between the force measuring plate and each ramp wooden board (Fig. 1(b)). The 10 mm gaps were designed to avoid undesired contact between the ramp wooden boards and the force plate. The force-measuring plate comprised one high-precision load sensor and two Q345 steel plates, as shown in Fig. 1(b). The data acquisition system (Fig. 1(c)) was used to record the signals transformed from the force-measuring plate system. To ensure that the foot is placed at the center of the force-measuring plate, a digital video camera was used to record each test and to identify whether the walking response would be useful for further vibration analysis. Therefore, only six among twelve traces in each walking test were selected to derive the walking force expression in this study.

Twenty-five volunteers participated in the walking force test. The test participants were instructed to walk through the force-measuring plate system (Fig. 1(d)) from a marked starting line. Each test participant walked forward and backward six times.

2.2. Walking force model

The typical load–time history under the walking excitation by Participant 1 is shown in Fig. 2(a). The one-step walking curve shown in Fig. 2(b) is similar to that of Harper's study [15]. Because the vertical vibration primarily controls the building floor's vibration serviceability, only the walking force in the direction of gravity is discussed herein.

The peak walking force (F_{max}) is associated with the walking posture, stride rate, and human weight in particular. A total of 150 traces (6 traces/participant × 25 participants) were acquired and used to calculate the ratios of the peak walking force (F_{max}) to the human weight (G). The ratios varied from 1.06 to 1.56, in which more than 85% of them were between 1.10 and 1.35, and the mean ratio (MEAN) was 1.2267 with a standard deviation (STD) of 0.1027 and a coefficient of variation (CV) of 0.0837, as shown in Fig. 2(c).

Additionally, T_p (Fig. 2(b)) which begins when the footfall touches the force-measuring plate and ends when the footfall leaves the force measuring plate completely, is another important vibration parameter. Fig. 2(d) shows the relationship between the ratio of the peak walking force to the human weight (F_{max}/G) and T_p. Moreover, more than 80% of the data were within the 15% error range (Fig. 2(d)), indicating a satisfactory distribution. Hence, a mean F_{max}/G of 1.2267 and a T_p of 0.6236 s were suggested for the walking vibration.

When conducting the theoretical analysis of the floor dynamic response due to walking excitation, G and T_p were considered; subsequently, the analysis was used to develop the walk forcing

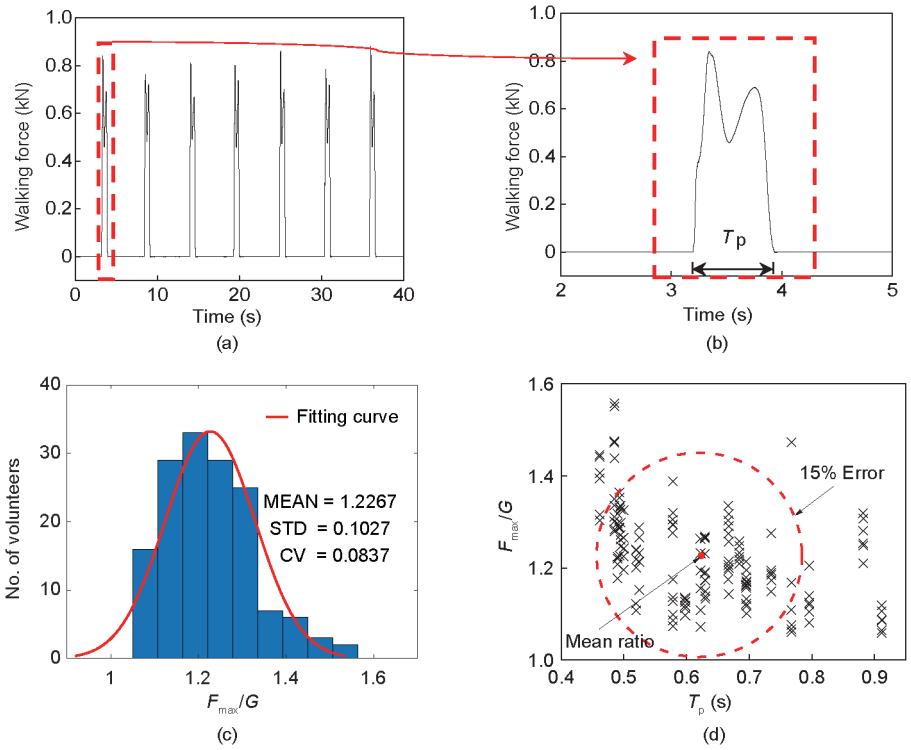

Fig. 2. Test results under the walking excitation. (a) Typical load–time history and (b) typical one-step curve of Participant 1; (c) distribution of the ratios of peak walking force (F_{max}) to the human weight (G); (d) relationship between F_{max}/G and T_p. MEAN: the mean ratio of the peak walking force (F_{max}) to the human weight (G); STD: the standard deviation for the ratio of the peak walking force (F_{max}) to the human weight (G); CV: the coefficient of variation for the ratio of the peak walking force (F_{max}) to the human weight (G).

function. The following Fourier series was used to define the one-step walk forcing function $F(t)$:

$$F(t) = G\left[\alpha_0 + \sum_{i=1}^{n} \alpha_n \sin\left(\frac{2\pi i}{T_p} t + \varphi_n\right)\right] \tag{3}$$

$$\alpha_0 = \frac{1}{G \times T_p} \int_0^{T_p} F(t)\mathrm{d}t \tag{4}$$

$$\alpha_n = \sqrt{A_n^2 + B_n^2} \tag{5}$$

$$\varphi_n = \arctan\left(\frac{A_n}{B_n}\right) \tag{6}$$

$$A_n = \frac{2}{G \times T_p} \int_0^{T_p} F(t)\cos\frac{2\pi n}{T_p} t\mathrm{d}t \tag{7}$$

$$B_n = \frac{2}{G \times T_p} \int_0^{T_p} F(t)\sin\frac{2\pi n}{T_p} t\mathrm{d}t \tag{8}$$

where n is the total number of contributing harmonics, α_n is the DLF, and φ_n is the phase angle. A_n and B_n are the Fourier coefficients.

Ebrahimpour and Hamam [21] stated that for walking activities, the higher-order harmonics (i.e., $n = 2$, $n = 3$, ...) were insignificant, particularly as the number of participants increased. As n increased, the simulation accuracy of the formulation increased, but more computations were incurred. Various orders of harmonics ($n = 1$–4) were considered in the formulation analysis, and the typical force–time histories from Participant 1 are shown in Fig. 3(a).

In comparison with the test results, Eq. (3) shows a better accuracy with $n = 2$, which yields a maximum error of 0.01% to −6.04%. Therefore, $F(t)$ can be modified as follows:

$$F(t) = G\left[\alpha_0 + \alpha_1 \sin\left(\frac{2\pi}{T_p} t + \varphi_1\right) + \alpha_2 \sin\left(\frac{4\pi}{T_p} t + \varphi_2\right)\right] \tag{9}$$

Based on the 150 walking tests, relationships between the DLFs (α_0, α_1, and α_2) and T_p, and those between the phase angles (φ_1 and φ_2) and T_p (based on Eq. (9)) can be established using the least-squares method. It is noteworthy that T_p ranged from 0.52 to 0.87 s. The main findings are as follows:

(1) As T_p increased, the coefficient α_0 decreased linearly, namely, $\alpha_0 = -0.2775T_p + 0.9799$, with an average α_0 of 0.790.

(2) As T_p increased, the coefficient α_1 increased linearly, that is, $\alpha_1 = 0.9246T_p - 0.4192$, with an average α_1 of 0.214.

(3) As T_p increased, the coefficient α_2 decreased linearly, that is, $\alpha_2 = -0.4616T_p + 0.6987$, with an average α_2 of 0.382.

(4) The linear correlation between the phase angle φ_1 (or φ_2) and T_p was unclear. However, the values of the phase angles (φ_1 and -0.5π) were primarily in the range of -0.5π to -0.3π.

(5) During the Fourier series expansion, the effect of the phase angle on the vibration periods was insignificant. However, the change in phase difference $\Delta\varphi(=\varphi_1 - \varphi_2)$ was important for determining the walking model. The value of $\Delta\varphi$ was predominantly 0, which may be assumed when defining the walking model. Hence, both φ_1 and φ_2 can be set as -0.5π for further analysis, which coincides with the values proposed by Chen et al. [19].

After determining the relationships among the force function parameters (i.e., the DLFs and phase angles in Eq. (9)) and T_p, the force–time responses were simulated using Eq. (9) and then plotted and compared with the test results. Typical fitted force–time curves were compared, as shown in Fig. 3(b). In all 150 groups of data, the maximum errors between the simulated and test results were less than 15%, with most of them being less than 10%. This suggests that Eq. (9) can be used to reasonably simulate the one-step walking force.

3. Vibration tests of CBHCS under walking

3.1. Test specimens

Seven full-scale tests were conducted on CBHCSs under walking. As indicated in Table 1, the beam span was either 6.0 m (four specimens) or 8.4 m (three specimens). The following two typical sizes of the H-shape steel beam were selected (depth × flange width × web thickness × flange thickness): 300 mm × 150 mm × 6.5 mm × 9 mm and 400 mm × 200 mm × 8.0 mm × 13 mm. Each H-shaped steel beam comprised two rows of headed shear studs measuring 19 mm (diameter) × 120 mm (height) pre-welded on its top flange (one row on each side of the flange). The transverse spacing of the studs was 50 mm, whereas different longitudinal spacings of 175, 280, and 475 mm were considered to reflect 100%, 70%, and 30% degrees of shear connection [22], respectively. The precast HCSs were placed on the top flanges of steel beams with a 25 mm bearing length, as shown in Fig. 1(a). Two floor widths of 2100 and 1800 mm were designed to investigate the effect of the floor width on the vibrational behavior of the CBHCS. To avoid concrete splitting between the headed shear studs (typically 19 mm in diameter and 120 mm long) and precast HCS (150 mm height), transverse tie reinforcements measuring 18 mm (diameter) × 1000 mm (total length of 450 mm in each HCS plus 100 mm gap) were inserted in the open cores of the HCSs at every 190 mm. To enhance the integrity of the composite beam

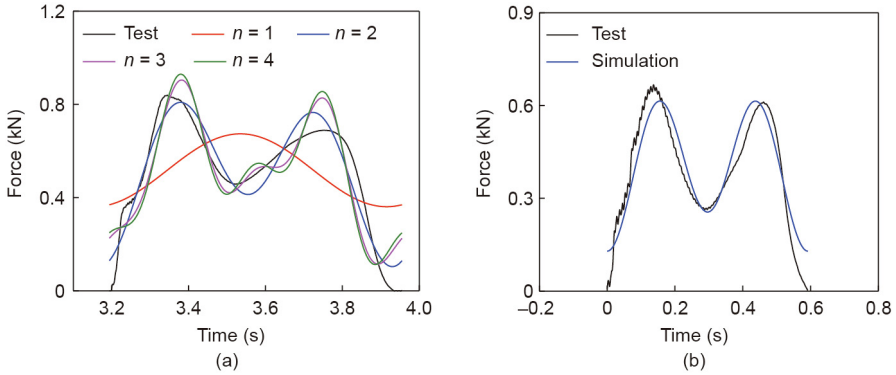

Fig. 3. Comparison of the walking force model (by Participant 1). (a) Comparisons between the measured and calculated curves for various orders of harmonics ($n = 1$–4) under the walking excitation; (b) comparisons of the fitted and test curves ($n = 2$).

Table 1
Details of the CBHCS specimens and test participants.

Specimen No.	Span (m)	Degree of shear connection	Floor width (mm)	Steel beam type	Participant No.	Weight (N)	Walking rate (Hz)
CBHCS-1	6.0	100%	2100	HN 300 × 150 × 6.5 × 9	1	590	1.67
CBHCS-2	8.4	100%		HN 400 × 200 × 8.0 × 13	2	610	1.87
CBHCS-3	8.4	30%		HN 400 × 200 × 8.0 × 13	3	590	1.69
CBHCS-4	8.4	70%		HN 400 × 200 × 8.0 × 13	4	710	2.00
CBHCS-5	6.0	30%		HN 300 × 150 × 6.5 × 9	5	500	1.82
CBHCS-6	6.0	70%		HN 300 × 150 × 6.5 × 9	6	540	1.81
CBHCS-7	6.0	100%	1800	HN 300 × 150 × 6.5 × 9	7	780	1.82

Steel beam type: depth (mm) × flange width (mm) × web thickness (mm) × flange thickness (mm).

and minimize walking noise, CIP concrete topping (60 mm thick) was added to the HCS. The gap between the HCSs was filled with *in-situ* concrete. In addition, mesh bars (diameter, 6 mm; spacing, 200 mm) were placed in the CIP concrete layer to avoid concrete cracking. The thickness of the CIP concrete layer was 60 mm. The complete details of the test specimens are presented in Table 1.

3.2. Test setup and instruments

Figs. 4(a)–(c) show schematic illustrations of the locations of accelerometers used for obtaining measurements from the transducers. The spacing between two adjacent accelerometers is clearly indicated for each direction. The monitoring system [23] comprised accelerometers (Type 2D001V, Jiangsu Donghua Testing Technology Co., Ltd., China) with an acceleration range of 2*g* and a data acquisition system (Model DH5922N, Jiangsu Donghua Testing Technology Co., Ltd.) (Figs. 4(d) and 1(c)).

This study focused on the vibration behavior of CBHCSs caused by walking impacts. For comparison, various walking rates were considered for the seven specimens (Table 1). Walking path A06–A07–A08–A09–A10 (Figs. 4(a)–(c)) was selected for each slab panel. Seven test participants were instructed to walk back and forth on each CBHCS for at least 60 s at the respective normal speed (Table 1), as shown in Fig. 4(e).

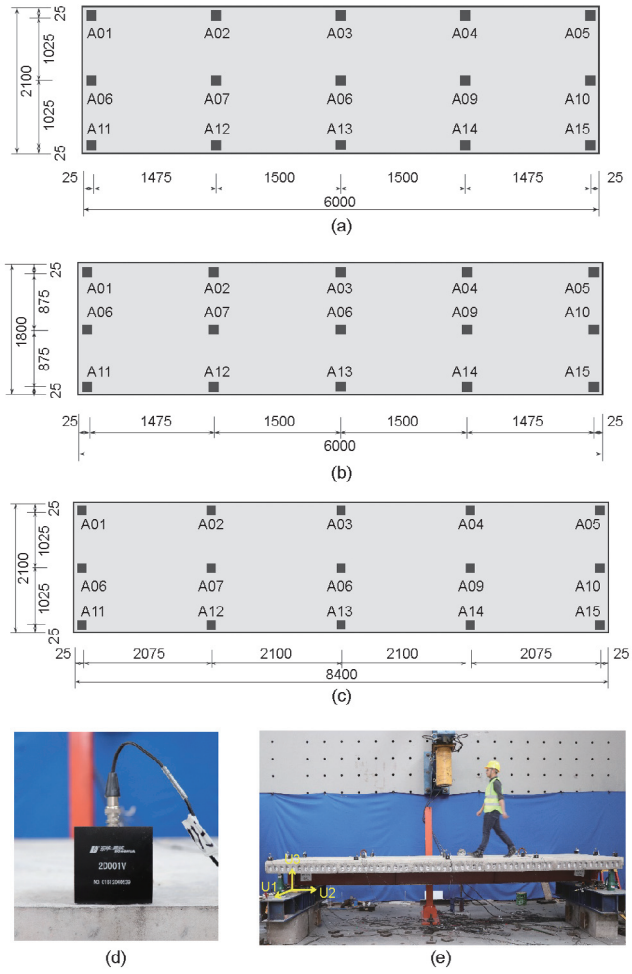

Fig. 4. Measurement locations and accelerometer numbering for (a) CBHCSs 1, 5, and 6, (b) CBHCS 7, and (c) CBHCSs 2, 3, and 4 (dimensions in mm); (d) the accelerometer (2D001V); and (e) the photo of walking test (U1 is perpendicular to U2 in horizontal direction, U2 is the horizontal walking direction, and U3 is the vertical direction).

3.3. Results and discussion

3.3.1. Acceleration in time domain

Typical acceleration traces at location A08 measured during the walking tests are shown in Fig. 5. All peak accelerations under walking excitation on each specimen are listed in Table 2. To quantify the human response to floor vibrations, ISO 2631-2 [24] lists the acceleration limits for mechanical vibrations, which are expressed in multiples of basic root–mean–square (RMS) accelerations. The RMS acceleration ($a_{\mathrm{RMS},i}$) can be calculated as follows:

$$a_{\mathrm{RMS},i} = \sqrt{\frac{a_i^2 + a_{i+1}^2 + \ldots + a_{i+N-1}^2}{N}} \tag{10}$$

where N is the number of data points considered during the integration period and a_i to a_{i+N-1} represent the individual accelerations. In this study, n was set to 1000 for an integration period of 1 s.

The peak RMS acceleration is referred to as the maximum transient vibration value (MTVV), which can be calculated as follows:

$$a_{\mathrm{MTVV}} = \max\{a_{\mathrm{RMS},i}\} \tag{11}$$

The average RMS acceleration (a_{ARMS}) can be calculated as follows:

$$a_{\mathrm{ARMS}} = \left(\sum_{i=1}^{n} a_{\mathrm{RMS},i}\right)/N \tag{12}$$

The peak and RMS accelerations at mid-span under walking impact are listed in Table 2, where χ_{rp} is the coefficient used to describe the relationship between the MTVV and peak acceleration, that is, $a_{\mathrm{MTVV}}/a_{\mathrm{peak}}$. The following are indicated in Table 2:

(1) No frequency weighting was used in this study. The degree of shear connection (100%, 70%, or 30%) did not significantly affect the vibrational frequency. Therefore, the stud connection may be disregarded when evaluating the vibrational serviceability of CBHCSs.

(2) The span and floor width of the specimen affected the vibrational behavior of the CBHCSs. Therefore, these parameters should be considered in the vibration evaluation.

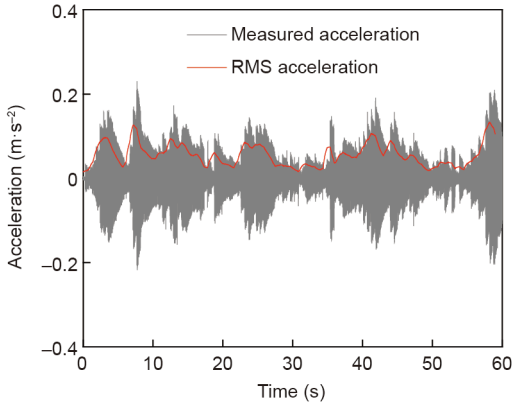

Fig. 5. Typical measured and root–mean–square (RMS) acceleration responses (Location A08 of CBHCS-7).

(3) χ_{rp} varied between 0.55 to 0.78. It is noteworthy that the average χ_{rp} coefficient was 0.58 for the CBHCSs under walking impact, calculated based on Grubbs' criterion [25].

3.3.2. Experimentally determined mode shapes

The mode shapes of the CBHCS floor system were extracted using the enhanced frequency domain decomposition (EFDD) method [26]. The first two mode shapes obtained from the experiments are shown in Fig. 6, where the first and second modes represent the typical bending and second-order bending shapes, respectively.

The representative experimentally obtained natural frequencies and damping ratios are listed in Table 2. The fundamental frequency for the 6.0 m-span specimens was approximately 16 Hz, which decreased to approximately 11.5 Hz when the span increased to 8.4 m. A damping ratio of 1% was suggested for further analysis.

4. Finite element analysis

4.1. Model details

The natural frequencies and mode shapes of the CBHCS were predicted using the general FE program ABAQUS [27]. The element of continuum stress/displacement three-dimensional with eight-node by reduced integration (C3D8R), the shell element with four-node by reduced integration (S4R), and the two-dimensional truss element of three-node piezoelectric (T3D2) were used to represent the concrete, steel beam, and reinforcements (or studs), respectively [28]. All material properties were determined based on the appropriate material tests. The elastic constants (elastic modulus of 3×10^4 MPa and Poisson's ratio of 0.2 for concrete; elastic modulus of 2×10^5 MPa and Poisson's ratio of 0.3 for steel) and density (7850 kg·m^{-3} for steel and 2400 kg·m^{-3} for concrete) were considered. A damping ratio of 1% was used in this study. The following boundary conditions were assumed to represent the simple support at each beam end: U1 = U2 = U3 = UR2 = UR3 = 0 and U1 = U3 = UR2 = UR3 = 0 (Fig. 4(e)). U1 = 0 means the translational degree of freedom (DOF) in the *x*-axis is 0 and UR1 = 0 means the rotational DOF about the *x*-axis is 0.

In the FE model, the floor was regarded as a solid instead of the HCS for simplicity and efficiency when using the S4R elements to model the floor. The h_{et} in Table 3 is the equivalent thickness of the solid floor with the same section inertia and mass as those of the CBHCS. The relationships between the h_{et} of the solid floor and the overall thickness *h* of the original CBHCS section are listed in Fig. 7 and Table 3.

4.2. Model validation

As shown in Fig. 8(a), the natural frequencies for the first two modes were similar between the FE analysis and test, with a relative error of less than 10% (Table 4). The following modal assurance criterion (MAC) [29] was used to identify the matching modes: $\mathrm{MAC}_{rs} = \left|\Phi_r^{\mathrm{T}}\tilde{\Phi}_s\right|^2 \Big/ \left[\left(\Phi_r^{\mathrm{T}}\tilde{\Phi}_r\right)\left(\Phi_s^{\mathrm{T}}\tilde{\Phi}_s\right)\right]$, where Φ_r is the identified testing mode (mode *r*) and $\tilde{\Phi}_s$ is the calculated mode (mode *s*). The MAC takes value between 0 (representing no consistent correspondence) and 1 (representing a consistent correspondence). MAC values larger than 0.9 indicate consistent correspondence whereas small values indicate poor resemblance of the two mode shapes. The MAC values for the first two modes generally exceed 0.95 (Table 4), indicating the high accuracy of the mode shapes from FE analysis.

A comparison of time histories is presented in Fig. 8(b), which shows that the relative error was less than 15% for peak accelerations and less than 10% for MTVVs. In summary, the FE model was validated and can be used for parametric studies.

4.3. Sensitivity study

Based on the test and FE analysis results, the natural frequencies and mode shapes of the CBHCSs with different shear connection degrees were similar for the first two modes. Hence, Specimen CBHCS-2 (*L* = 8.4 m, the tested acceleration a_{test}) was selected to conduct the parametric study. A total of 20 FE analyses were conducted by varying one parameter at each time to further investigate the effects of different factors on the vibrational behavior of the CBHCSs. The walking frequency was set to 2.0 Hz. The primary factors included the floor thickness, steel beam type, contact time, and human weight. The FE analyses are summarized in Table 5 and Fig. 9.

Taking CBHCS-205-400-0.72-610 as an example to explain the designation: 205 is the equivalent floor thickness in mm; 400 indicates the steel beam HN 400 × 200 × 8 × 13 having a depth of

Table 2
Testing result comparison.

Specimen No.	Length (m)	Width (m)	Tester weight (kg)	Degree of shear connection	a_{peak} (mm·s^{-2})	a_{MTVV} (mm·s^{-2})	χ_{rp}	Frequency (Hz)		Damping ratio (%)	
								1st	2nd	1st	2nd
CBHCS-1	6.0	2.1	59	100%	65.1	25.4	0.78	16.07	52.69	0.71	0.90
CBHCS-2	8.4	2.1	61	100%	127.4	71.9	0.56	11.48	38.66	0.87	0.60
CBHCS-3	8.4	2.1	59	30%	84.4	53.7	0.64	11.31	37.55	1.23	0.50
CBHCS-4	8.4	2.1	71	70%	117.7	67.5	0.57	11.70	32.55	1.27	0.90
CBHCS-5	6.0	2.1	50	30%	138.4	77.2	0.56	15.92	49.91	1.24	0.80
CBHCS-6	6.0	2.1	54	70%	142.9	78.3	0.55	15.79	48.89	0.93	1.40
CBHCS-7	6.0	1.8	78	100%	230.2	132.6	0.58	16.67	50.92	1.03	2.20

a_{MTVV}: the maximum transient vibration value; a_{peak}: the peak acceleration; χ_{rp}: the coefficient used to describe the relationship between a_{MTVV} and a_{peak} (i.e., a_{MTVV}/a_{peak}).

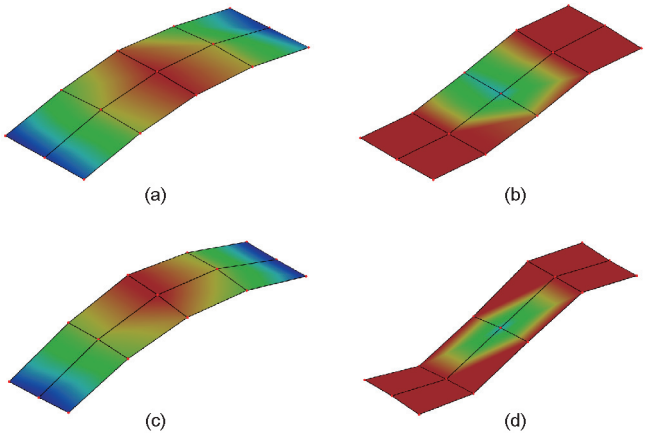

Fig. 6. Representative experimentally obtained mode shapes. (a, b) First mode shape (16.07 Hz) and second mode shape (52.69 Hz) of Specimen CBHCS-1 (6.0 m-span); (c, d) first mode shape (11.48 Hz) and second mode shape (38.66 Hz) of Specimen CBHCS-2 (8.4 m-span).

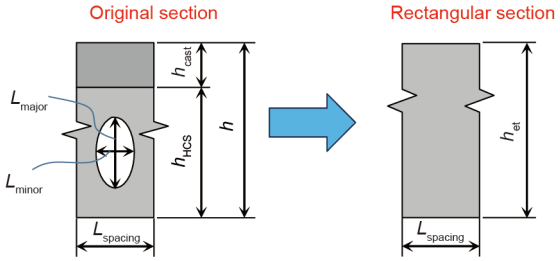

Fig. 7. Transformed Area Method. h_{HCS}: the thickness of HCS floor; h_{cast}: the thickness of cast *in-situ* floor; L_{major}: length of major axis of elipse; L_{minor}: length of minor axis of elipse; $L_{spacing}$: the hole spacing of CBHCS.

400 mm; 0.72 is the contact time in second; and 610 is the weight of test participant in N.

The main FE analysis results are discussed as follows.

4.3.1. Floor thickness

The effect of the h_{et} on the natural frequency and acceleration response was investigated by varying the h_{et} values (150–205 mm), as shown in Tables 3 and 5. The calculated fundamental and second-order frequencies increased slowly with h_{et} as the bending stiffness increased (Fig. 9(a)). In addition, the peak acceleration, MTVV, and the average RMS (ARMS) increased with h_{et}, particularly when h_{et} > 195 mm (Fig. 9(b)). Because the opening ratio of the HCS increases with h_{et}, local vibrations will occur when the opening ratio of the HCS is increased; this will result in greater vibrational responses, which should be focused upon in vibration analysis.

4.3.2. Steel beam type

The effect of the steel beam type on the natural frequency and acceleration response was investigated by changing the arrangement of the steel beam, as shown in Table 5. Four different steel beam arrangements were investigated and compared. The calculated fundamental and second-order frequencies increased with the steel beam height (h_{beam}) because the bending stiffness increased (Fig. 9(c)). Fig. 9(d) shows that the peak acceleration, MTVV, and ARMS were affected significantly when $h_{beam} \leq 400$ mm, whereas these values decreased significantly when $h_{beam} > 400$ mm owing to the increasing mass and stiffness of the specimen.

4.3.3. Contact time T_P

The effects of T_p on the natural frequency and acceleration response were investigated, as shown in Table 5. The natural frequencies of the first two modes were barely affected because T_p contributed insignificantly to the floor stiffness and mass (Fig. 9(e)). T_p did not affect the stiffness or mass of the structure, as the applied walking forces using T_p did not interfere with the floor natural frequencies. When T_p increased, the peak acceleration, MTVV, and ARMS decreased owing to the decreasing impact force (Fig. 9(f)).

4.3.4. Human weight

The effect of human weight (505, 610, 681, 812, and 900 N) on the natural frequency and acceleration response was investigated, as shown in Table 5. The natural frequencies of the first two vibration modes were barely affected because G contributed insignificantly to the floor stiffness and mass (Fig. 9(g)). G did not affect the stiffness or mass of the structure, as the applied walking forces using G did not interfere with the floor natural frequencies. Fig. 9(h) shows that as G increased, the peak acceleration, MTVV, and ARMS increased with the impact force.

5. Evaluation of vibration serviceability of CBHCS

5.1. Frequency

A simply supported beam subjected to dynamic loading is shown in Fig. 10(a), where the important beam properties are the flexural stiffness EI (E is the elastic modulus; I is the area moment of inertia of the beam cross-section about the axis of interest) and the mass per unit length $\overline{m}$, both assumed to be constant along the span L. The transverse loading force $F(x,t)$ varies with position and time, resulting in various transverse-displacement responses $v(x,t)$.

For free vibrations, that is, $F(x,t) = 0$, the equation becomes

Table 3
Relationships between the equivalent thickness h_{et} of the solid floor and thickness h of the original CBHCS section.

The overall thickness of the composite floor $h = h_{HCS} + h_{cast}$ (mm)	The thickness of HCS floor h_{HCS} (mm)	The thickness of cast *in-situ* floor h_{cast} (mm)	Length of major axis of ellipse L_{major} (mm)	Length of minor axis of ellipse L_{minor} (mm)	The hole spacing of CBHCS $L_{spacing}$ (mm)	The equivalent thickness h_{et} (mm)
155	95	60	70	57	95	150
165	105	60	75	57	95	160
175	115	60	80	57	95	170
185	125	60	80	57	95	180
195	135	60	85	57	95	190
200	140	60	90	57	95	195
205	145	60	95	57	95	200
215	150	60	95	57	95	205

$$EI\frac{\partial^4 v(x,t)}{\partial x^4}+\overline{m}\frac{\partial^2 v(x,t)}{\partial t^2}=0 \tag{13}$$

If $v(x,t)=\phi(x)Y(t)$, then

$$\frac{\phi^{\mathrm{iv}}(x)}{\phi(x)}+\frac{\overline{m}}{EI}\frac{Y(t)}{Y(t)}=0 \tag{14}$$

where iv in the superscripts means the fourth derivative. $Y(t)$ means the time related displacement responses. $\phi(x)$ means the position related displacement responses.

If $\frac{\phi^{\mathrm{iv}}(x)}{\phi(x)}=-\frac{\overline{m}}{EI}\frac{\ddot{Y}(t)}{Y(t)}=a^4=\frac{\omega^2\overline{m}}{EI}$ and the following boundary conditions are imposed

$$\phi(L)=0, M(L)=EI\phi''(L)=0 \tag{15}$$

where $M(0)$ or $M(L)$means the bending moment at $x=0$ or $x=L$.

Then

$$\phi(x)=\Omega\sin ax \tag{16}$$

where Ω is the coefficient.

Because $\phi(L)=0$, Ω,

$$a=n\pi/L(n=0,1,2,\ldots) \tag{17}$$

Therefore, the natural frequencies can be calculated as follows:

$$f_n=\frac{\omega_n}{2\pi}=\frac{n^2\pi^2\sqrt{\frac{EI}{\overline{m}L^4}}}{2\pi}=\frac{n^2\pi}{2}\sqrt{\frac{EI}{\overline{m}L^4}} \tag{18}$$

where ω_n is the circular frequency.

Using the theory above, the theoretical fundamental frequency (n = 1) of the specimens can be obtained. Table 6 shows a compari-

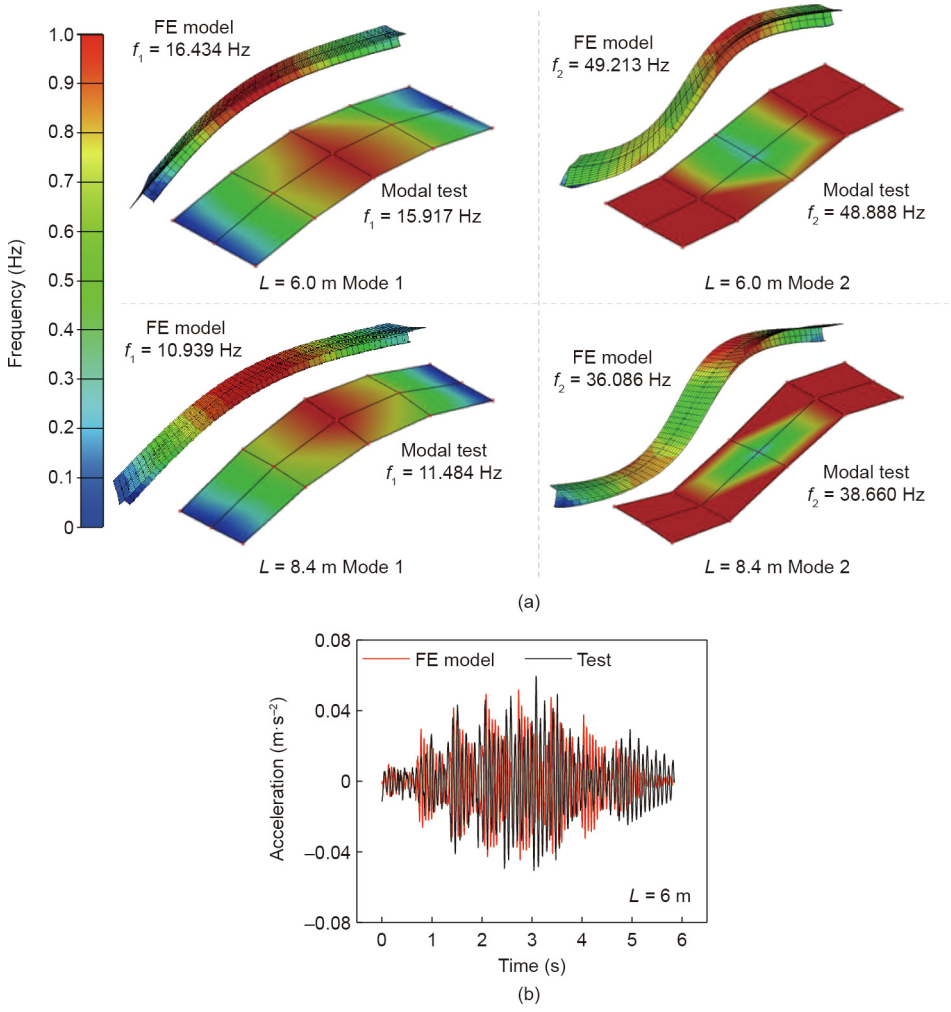

Fig. 8. Model validation. (a) Comparison of natural frequencies between the FE analysis and test; (b) comparison of acceleration histories between the FE analysis and test (CBHCS-1). L: the beam span.

Table 4
Comparison of natural frequencies and modal assurance criterion values (MACs).

Specimen	Mode	FE model (Hz)	Modal test (Hz)	Error (%)	MAC
CBHCS-1	1	16.434	15.917	3.15	0.98
	2	49.213	48.888	0.66	0.95
CBHCS-2	1	10.939	11.484	4.75	0.99
	2	36.086	38.660	6.66	0.96

Table 5
Summary of the FE analyses.

FE model No.	h_{et} (mm)	Steel beam type	Contact time T_P (s)	Human weight G (N)
CBHCS-205-400-0.72-610	205	HN 400 × 200 × 8.0 × 13	0.72	610
CBHCS-150-400-0.72-610	150	HN 400 × 200 × 8.0 × 13	0.72	610
CBHCS-160-400-0.72-610	160			
CBHCS-170-400-0.72-610	170			
CBHCS-180-400-0.72-610	180			
CBHCS-190-400-0.72-610	190			
CBHCS-195-400-0.72-610	195			
CBHCS-200-400-0.72-610	200			
CBHCS-205-250-0.72-610	205	HN 250 × 200 × 6.0 × 9	0.72	610
CBHCS-205-300-0.72-610		HN 300 × 150 × 6.5 × 9		
CBHCS-205-450-0.72-610		HN 450 × 200 × 9.0 × 14		
CBHCS-205-400-0.63-610	205	HN 400 × 200 × 8.0 × 13	0.63	610
CBHCS-205-400-0.65-610			0.65	
CBHCS-205-400-0.69-610			0.69	
CBHCS-205-400-0.76-610			0.76	
CBHCS-205-400-0.83-610			0.83	
CBHCS-205-400-0.72-505	205	HN 400 × 200 × 8 × 13	0.72	505
CBHCS-205-400-0.72-681				681
CBHCS-205-400-0.72-812				812
CBHCS-205-400-0.72-900				900

son between the theoretical and test results. As shown, the relative errors were generally less than 7%. Hence, the fundamental frequency, calculated using Eq. (18), was considered acceptable.

5.2. Acceleration

The equation of motion of a single-degree-of-freedom (SDOF) system can be reduced to the following form:

$$m\ddot{v}(t) + c\dot{v}(t) + kv(t) = F(t) \tag{19}$$

where t is the time, m is the mass of vibration, c the viscous damping coefficient, k the stiffness, $v(t)$ the displacement of the mass, and $F(t)$ the force applied to the mass. In this study, it is assumed that the system shown in Fig. 10(b) is subjected to a harmonically varying load $F(t)$ of amplitude F_0 and circular frequency ϖ. In this case, the differential equation of motion becomes

$$m\ddot{v}(t) + c\dot{v}(t) + kv(t) = F_0\cos(\varpi t) \tag{20}$$

As $\frac{c}{m} = 2\beta\omega$ (β is the damping ratio) and $\frac{k}{m} = \omega^2$, the following is obtained:

$$\ddot{v}(t) + 2\beta\omega\dot{v}(t) + \omega^2 v(t) = \frac{F_0}{m}\cos(\varpi t) \tag{21}$$

The solution of Eq. (21) can be expressed as

$$v(t) = Ae^{-\beta\omega t}\sin(\omega_d t + \varphi') + \mu\cdot\frac{F_0}{k}\cos(\varpi t - \varphi) \tag{22}$$

where the amplitude $A = \sqrt{v(0)^2 + \frac{[\dot{v}(0)+\beta\omega v(0)]^2}{\omega_d^2}}$, the oscillatory circular frequency $\omega_d = \omega\sqrt{1-\beta^2}$, $\varphi' = \tan^{-1}\frac{\omega_d\cdot v(0)}{\dot{v}(0)+\beta\omega v(0)}$, $\varphi = \tan^{-1}\frac{2\beta\omega}{1-\xi^2}$, the magnification factor $\mu = \frac{1}{\sqrt{(1-\xi^2)^2+(2\beta\omega)^2}}$, and the circular frequency ratio $\xi = \frac{\varpi}{\omega}$.

In Eq. (22), the first term $Ae^{-\beta\omega t}\sin(\omega_d t + \varphi')$ represents the transient response, which vanishes rapidly with damping and is negligible, thereby yielding an acceleration expressed as follows:

$$\ddot{v}(t) = \varpi^2\mu\cdot\frac{F_0}{k}\cos(\varpi t - \varphi) \tag{23}$$

The peak acceleration is expressed as

$$a_{peak} = \varpi^2\mu\cdot\frac{F_0}{k} \tag{24}$$

where $F_0 = \alpha G$, $\varpi = \omega = \sqrt{\frac{k}{m}}$, and $\mu = \frac{1}{2\beta}$. The AISC Design Guide 11 [30] recommends 700 N for the human weight G.

The coefficient α is calculated as follows:

$$\alpha = 0.83e^{-0.35f_1} \tag{25}$$

a_{peak} can be re-expressed as

$$a_{peak} = \frac{0.83e^{-0.35f_1}G}{2\beta m} \tag{26}$$

where $m = \rho\overline{m}L$ and the boundary coefficient $\rho = 0.5$ represent simple supports. In this study, the human mass was assumed to be 65 kg (i.e., G = 650 N), based on the walking force measurements discussed in Section 2. The calculated peak accelerations based on the equation of motion for an SDOF system were compared with those from the tests, and a relative error less than 50% was indicated (Table 6). Acceptable results are achievable if the actual walking force is employed to calculate the acceleration response of each specimen using the FE method. However, it is unrealistic to perform further floor vibration evaluations using the actual walking force each time. A unified walking force (i.e., coefficient $\alpha \times G$) is typically used to obtain the peak acceleration. Therefore, an error less than 50% (Table 6) is considered acceptable.

The relationship between the MTVV and peak acceleration can be expressed as

$$a_{MTVV} = \chi_{rp}a_{peak} \tag{27}$$

The average χ_{rp} coefficient was calculated to be 0.58, compared with 0.2 reported by Zhou et al. [31]. As shown in Table 6, the relative error of the calculated MTVVs was 6% on average and 41% at the maximum. Better results can be obtained if the actual walking forces are employed to calculate the acceleration response of each specimen. In general, the applied walking force should be calculated using Eq. (9). Therefore, the calculated force cannot truly reflect the walking posture or the actual vibration response. Furthermore, the thresholds of floor vibration specified in AISC Design Guide 11 [30] are 50, 150, and 500 mm·s^{-2} for different types of floors. This implies that the order of magnitude for accelerations, instead of the actual acceleration value, is typically used in floor vibration evaluations. Hence, the MTVVs calculated using Eq. (27) were considered acceptable.

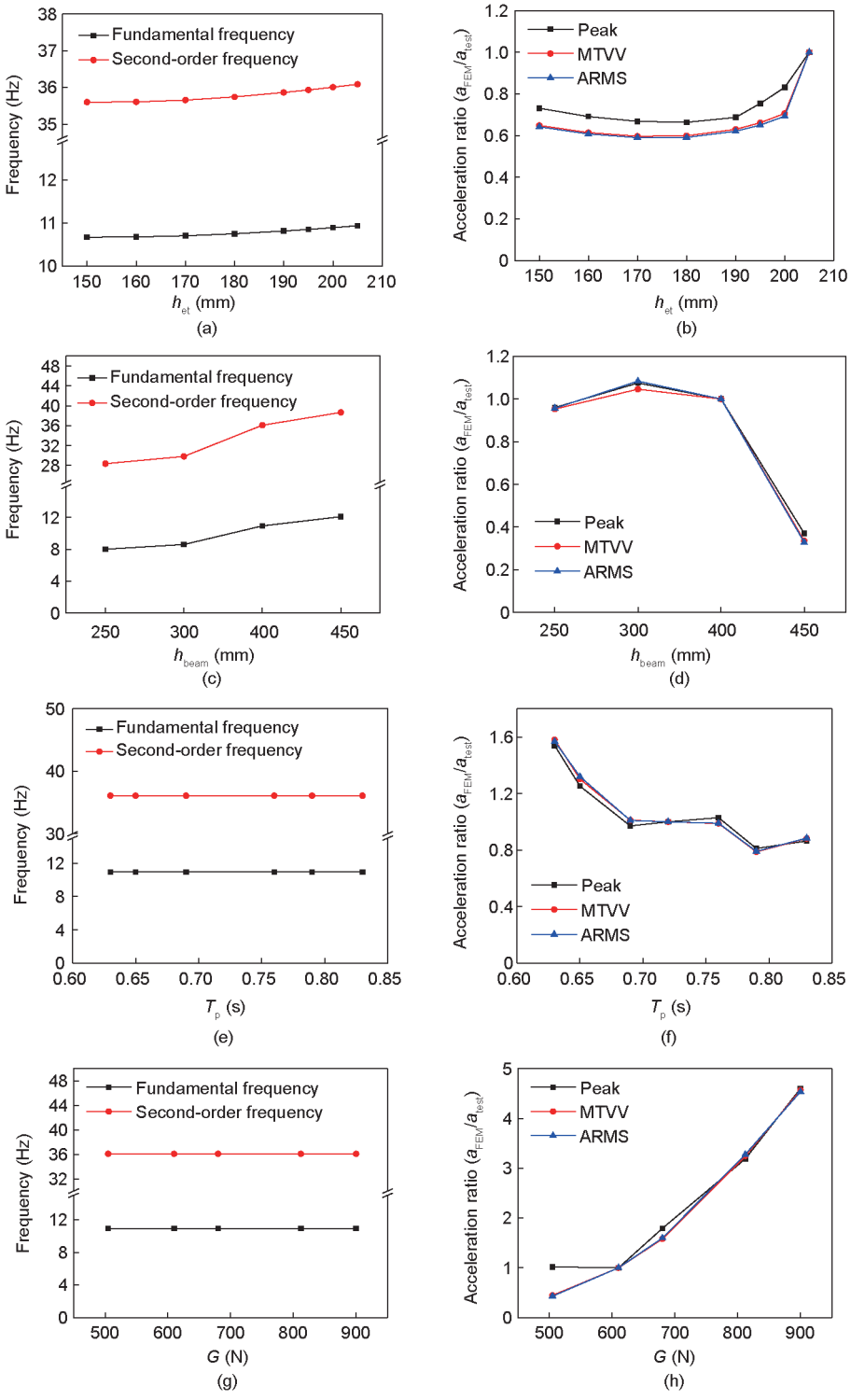

Fig. 9. Parametric analysis results of the CBHCS. Effects of (a, b) floor thickness, (c, d) steel beam type, (e, f) contact time, and (g, h) human weight on frequency and acceleration, respectively. a_{FEM} is the acceleration value calculated from the FE method; a_{test} is the measured acceleration value; h_{beam}: the steel beam height; ARMS: the average RMS.

6. Conclusions

In this study, 150 load–time histories from walking were obtained using a force measuring plate. Vibration tests on seven CBHCS specimens were conducted in addition to theoretical analysis. This study focused on the behavior in the vicinity of the steel beam and the vibratory motion of a steel–concrete CBHCS. On a real floor, vibrations occur at the center of the slab and should be addressed in future studies. The following conclusions were obtained from this study:

(1) The ratio of peak walking force to human weight ranged from 1.10 to 1.35. A Fourier series walking function with n = 2 was derived, that is, Eq. (9). Relationships between the function parameters (DLFs and phase angles) with T_p were determined as follows: $\alpha_0 = -0.2775T_p + 0.9799$, $\alpha_1 = 0.9246T_p - 0.4192$, and $\alpha_2 = -0.4616T_p + 0.6987$; and $\varphi_1 = \varphi_2 = -\pi/2$. A mean F_{max}/G

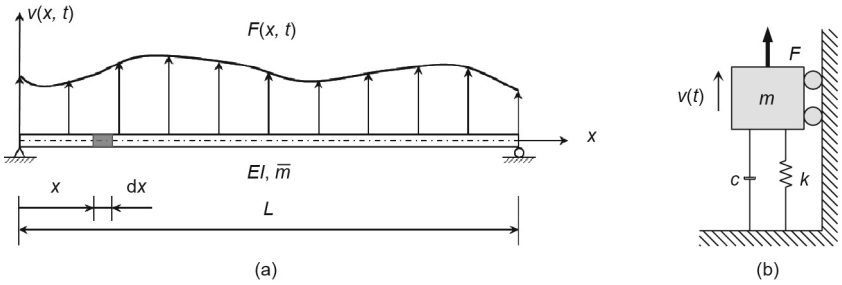

Fig. 10. Theory analysis models. (a) Simple beam subjected to dynamic loading; (b) a single-degree of freedom (SDOF) system.

Table 6
Comparison of the fundamental frequencies and accelerations.

Specimen No.	Span (m)	Floor width (m)	G (N)	Modal test f_1 (Hz)	Eq. (18) results f_1 (Hz)	Error (%)	Test a_{peak} (mm·s^{-2})	$a_{peak(26)}$ by Eq. (26) (mm·s^{-2})	$a_{peak(26)}$/a_{peak}	Error between $a_{peak(26)}$ and a_{peak}	a_{MTVV} (mm·s^{-2})	$a_{MTVV(27)}$ by Eq. (27) (mm·s^{-2})	$a_{MTVV(27)}$/a_{MTVV}	Error between $a_{MTVV(27)}$ and a_{MTVV}
CBHCS-1	6.0	2.1	590	16.07	16.33	1.62	65.10	95.00	146%	46%	50.80	54.60	107%	7%
CBHCS-2	8.4	2.1	610	11.48	10.97	−4.44	127.40	101.27	79%	−21%	71.90	58.20	81%	−19%
CBHCS-3	8.4	2.1	590	11.31	10.97	−3.01	84.40	103.96	123%	23%	53.70	59.75	111%	11%
CBHCS-4	8.4	2.1	710	11.70	10.97	−6.24	117.70	109.14	93%	−7%	67.50	62.72	93%	−7%
CBHCS-5	6.0	2.1	500	15.92	16.33	2.58	69.20	84.85	123%	23%	38.60	48.76	126%	26%
CBHCS-6	6.0	2.1	540	15.79	16.33	3.42	71.45	95.90	134%	34%	39.15	55.12	141%	41%
CBHCS-7	6.0	1.8	780	16.67	16.71	0.24	115.10	95.24	83%	−17%	66.30	54.73	83%	−17%

ratio of 1.2267 and T_p of 0.6236 s were suggested for the walking vibration on the CBHCS floor.

(2) The CBHCS floor system indicated a high frequency (> 10 Hz) and low damping (~1%). The mode shapes predicted from the FE analysis matched those from the tests. The CBHCS floor exhibited flexural mode shapes during human walking.

(3) FE analyses indicated that the primary factors affecting the vibration of the CBHCS floor were the floor thickness, steel beam type, contact time (T_P), and human weight (G). However, T_p and G barely affected the natural frequencies of the first two vibration modes because they contributed insignificantly to the floor stiffness and mass. This is because T_p and G did not affect the stiffness or mass of the structure, as they were applied forces that did not interfere with the natural frequencies.

(4) The theoretical fundamental frequency of the CBHCS floor can be obtained using beam vibration theory. The relative errors were generally less than 6%, indicating that the fundamental frequency calculated using Eq. (18) was reasonably accurate.

(5) The calculated peak accelerations based on the equation of motion for an SDOF system were compared with those from the tests, and a relative error less than 50% was indicated. An average χ_{rp} coefficient of 0.58 was suggested to obtain the MTVV. The MTVV result (maximum error less than 50%) is acceptable because the order of magnitude of the accelerations instead of the actual acceleration value is typically used in floor vibration evaluations.

Acknowledgment

The authors acknowledge the financial support provided by the National Natural Science Foundation of China (51890902 and 51708058).

Compliance with ethics guidelines

Jiepeng Liu, Shu Huang, Jiang Li, and Y. Frank Chen declare that they have no conflict of interest or financial conflicts to disclose.

References

[1] Girhammar UA, Pajari M. Tests and analysis on shear strength of composite slabs of hollow core units and concrete topping. Constr Build Mater 2008;22(8):1708–22.
[2] Ibrahim IS, Elliott KS, Abdullah R, Kueh ABH, Sarbini NN. Experimental study on the shear behaviour of precast concrete hollow core slabs with concrete topping. Eng Struct 2016;125:80–90.
[3] Baran E. Effects of cast-in-place concrete topping on flexural response of precast concrete hollow-core slabs. Eng Struct 2015;98:109–17.
[4] Kankeri P, Prakash SS. Experimental evaluation of bonded overlay and NSM GFRP bar strengthening on flexural behavior of precast prestressed hollow core slabs. Eng Struct 2016;120:49–57.
[5] Lam D, Elliott KS, Nethercot DA. Steel-concrete composite construction with precast concrete hollow core floor. In: Proceedings of The Second International Conference on Advances in Steel Structures; 1999 Dec 15–17; Hong Kong, China. Amsterdam: Elsevier; 1999. p. 459–66.
[6] Lam D, Elliott KS, Nethercot DA. Experiments on composite steel beams with precast concrete hollow core floor slabs. Proc Inst Civ Eng, Struct Build 2000;140(2):127–38.
[7] Lam D, Elliott KS, Nethercot DA. Parametric study on composite steel beams with precast concrete hollow core floor slabs. J Construct Steel Res 2000;54(2):283–304.
[8] Lam D, Nip TF. Effects of transverse reinforcement on composite beam with precast hollow core slabs. In: Proceedings of the Third International Conference on Advances in Steel Structures; 2002 Dec 9–11; Hong Kong, China. Amsterdam: Elsevier; 2002. p. 503–10.
[9] Lam D. Capacities of headed stud shear connectors in composite steel beams with precast hollowcore slabs. J Construct Steel Res 2007;63(9):1160–74.
[10] Aguado JV, Espinos A, Hospitaler A, Ortega J, Romero ML. Influence of reinforcement arrangement in flexural fire behavior of hollow core slabs. Fire Saf J 2012;53:72–84.
[11] Aguado JV, Albero V, Espinos A, Hospitaler A, Romero ML. A 3D finite element model for predicting the fire behavior of hollow-core slabs. Eng Struct 2016;108:12–27.
[12] Jendzelovsky N, Zabakova Vrablova K. Comparison of natural frequencies of hollow core slabs. Appl Mech Mater 2015;769:225–8.
[13] Marcos LK, Carrazedo R. Parametric study on the vibration sensitivity of hollow-core slabs floors. In: Proceedings of the 9th International Conference on Structural Dynamics, EURODYN 2014; 2014 Jun 30–Jul 2; Porto, Portugal. p. 1095–102.
[14] Liu F, Battini JM, Pacoste C, Granberg A. Experimental and numerical dynamic analyses of hollow core concrete floors. Structures 2017;12:286–97.
[15] Harper FC. The mechanics of walking. Res Appl Ind 1962;15(1):23–8.
[16] Blanchard J, Davies BL, Smith JW. Design criteria and analysis for dynamic loading of footbridges. In: Proceeding of a Symposium on Dynamic Behaviour of Bridges at the Transport and Road Research Laboratory; 1977 May 19; Crowthorne, England. Washington, DC: TRID; 1977. p. 90–106.

[17] Allen DE, Murray TM. Design criterion for vibrations due to walking. Eng J 1993;30(4):117–29.
[18] Živanović S, Pavić A, Reynolds P. Probability-based prediction of multi-mode vibration response to walking excitation. Eng Struct 2007;29(6):942–54.
[19] Chen J, Peng Y, Wang L. Experimental investigation and mathematical modeling of single footfall load using motion capture technology. China Civil Eng J 2014;47(3):79–87. Chinese.
[20] Chen J, Ding G, Živanović S. Stochastic single footfall trace model for pedestrian walking load. Int J Struct Stab Dyn 2019;19(03):1950029.
[21] Ebrahimpour A, Hamam A, Sack RL, Patten WN. Measuring and modeling dynamic loads imposed by moving crowds. J Struct Eng 1996;122(12):1468–74.
[22] EN 1994-1-1. Euro Code 4. Design of composite steel and concrete structures-Part 1-1: General rules and rules for buildings. European standard. Brussels: European Committee for Standardization; 2004.
[23] DHDAS software [Internet]. Jingjiang: Donghua Testing Technology; c2021 [cited 2020 Sep 29]. Available from: http://www.dhtest.com/dhdasrj.
[24] ISO 2631-2. Mechanical vibration and shock-Evaluation of human exposure to whole-body vibration—part 2: vibration in buildings (1 Hz to 80 Hz). ISO standard. Geneva: International Organization for Standardization; 2003.
[25] Grubbs FE. Procedures for detecting outlying observations in samples. Technometrics 1969;11(1):1–21.
[26] Altunişik AC, Bayraktar A, Sevim B, Özdemir H. Experimental and analytical system identification of Eynel arch type steel highway bridge. J Construct Steel Res 2011;67(12):1912–21.
[27] Abaqus, Inc. Abaqus analysis user's manual version 6.14. Boston: Dassault Systemes Simulia Corp., USA; 2014.
[28] Bai J, Chen H, Zhao J, Liu M, Jin S. Seismic design and subassemblage tests of buckling-restrained braced RC frames with shear connector gusset connections. Eng Struct 2021;234:112018.
[29] Li J, Zhang R, Liu J, Cao L, Chen YF. Determination of the natural frequencies of a prestressed cable RC truss floor system. Measurement 2018;122:582–90.
[30] Murray T, Allen D, Ungar E, Davis DB. Floor vibrations due to human activities: design guide 11. 2nd ed. Chicago: American Institute of Steel Construction; 2016.
[31] Zhou X, Cao L, Chen YF, Liu J, Li J. Experimental and analytical studies on the vibration serviceability of pre-stressed cable RC truss floor systems. J Sound Vibrat 2016;361:130–47.